

Superfluid helium film may greatly increase the storage time of ultracold neutrons in material traps

P. D. Grigoriev^{1,2} and A. M. Dyugaev¹

¹*L. D. Landau Institute for Theoretical Physics, Chernogolovka, Moscow region, 142432, Russia*

²*National University of Science and Technology MISiS, 119049, Moscow, Russia**

(Dated: November 16, 2021)

We propose a method to increase both the neutron storage time and the precision of its lifetime measurements by at least tenfold. The storage of ultracold neutrons (UCN) in material traps now provides the most accurate measurements of neutron lifetime and is used in many other experiments. The precision of these measurements is limited by the interaction of UCN with the trap walls. We show that covering of trap walls with liquid helium may strongly decrease the UCN losses from material traps. ⁴He does not absorb neutrons at all. Superfluid He covers the trap walls as a thin film, ~ 10 nm thick, due to the van der Waals attraction. However, this He film on a flat wall is too thin to protect the UCN from their absorption inside a trap material. By combining the van der Waals attraction with capillary effects we show that surface roughness may increase the thickness of this film much beyond the neutron penetration depth ~ 33 nm. Using liquid He for UCN storage requires low temperature $T < 0.5$ to avoid neutron interaction with He vapor, while the neutron losses because of the interaction with surface waves are small and can be accounted for using their linear temperature dependence.

I. INTRODUCTION

Slow neutrons play an important role in particle physics, both as a tool and an object. The properties of a free neutron and its interactions with known or hypothetical fields provide a valuable information about fundamental particles and interactions.[1–5] The precise measurements of neutron lifetime τ_n are important for elementary particle physics, astrophysics and cosmology (see [1–5] for reviews). The search for a non-vanishing electric dipole moment of neutrons[6–8] impose the limits on CP violation. Precise measurements of a β -decay asymmetry provide information on axial-vector weak coupling constant [9–11]. The resonant transitions between discrete quantum energy levels of neutrons in the earth gravitational field[12, 13] probe the gravitational field on a micron length scale and impose constraints on dark matter.

A large class of experiments employs neutrons with energy lower than the neutron optical potential of typical materials, i.e. $\lesssim 300$ neV [7, 8, 10–12, 14–21]. These so-called ultracold neutrons (UCNs) can be trapped for many minutes in well-designed "neutron bottles"[17–21]. The gravitational interaction with a potential difference of 100 neV per meter rise plays important role in UCN storage and manipulation[14–20]. Because of the neutron magnetic moment of 60 neV/T, magneto-gravitational trapping of UCN is feasible too[22–26].

The main alternative to using UCN in neutron lifetime measurements is the cold neutron beam[27–29], giving $\tau_n = (887.7 \pm 1.2[\text{stat}] \pm 1.9[\text{syst}])\text{s}$. Using UCN in τ_n measurements is believed to be much more precise. Therefore, according to the Particle Data Group, the conventional neutron lifetime value $\tau_n = 879.4 \pm 0.6$ s is only based on the UCN experiments [17, 18, 20, 25, 26]. The discrepancy between these two methods is far beyond the estimated error. This "neutron lifetime puzzle" is a subject of ex-

tensive discussion till now[29–32]. Presumably, it is due to unconsidered systematic errors in beam experiments[32], but their origin is not understood yet. Other possibilities involving new physics, such as additional neutron decay channels or dark matter [29, 30], most probably, are not the reason for this discrepancy, as was shown by analyzing the neutron β -decay asymmetry [33]. The accuracy of current UCN lifetime measurements also requires additional analysis, because unconsidered or underestimated systematic errors in UCN experiments are also possible.

The main problem with the UCN is their storage. The traditional materials for UCN trap walls are[15] beryllium, beryllium oxide, nickel, diamond-like carbon, copper, aluminium and others. They have low neutron loss coefficient η and high potential barrier V_0 for UCN. For beryllium the theoretical value of loss coefficient $\eta \sim 10^{-6} - 10^{-5}$ depending on temperature[14] and the potential barrier $V_0^{Be} = 252$ neV. The corresponding neutron penetration depth into Be is $\kappa_{0Be}^{-1} = \hbar/\sqrt{2mV_0^{Be}} \approx 9$ nm, where the neutron mass $m = 1.675 \times 10^{-24}$ g. The first experiments with UCN material traps were discouraging and demonstrated too short neutron storage time of few minutes.[14, 15] The origin of such strong neutron losses was puzzling for more than a decade. Finally these losses were shown to originate mainly from inelastic neutron scattering because of surface contamination by hydrogen[34] (see also [14, 15] for a review). Various methods were applied to reduce the surface contamination.[14, 15] For example, the material traps were equipped with sputtering heads, enabling fresh surfaces on the walls which had never been exposed to the atmosphere. This improvement finally reduced the systematic error in τ_n to ~ 10 s in Be or Al traps with surface covered with heavy water or oxygen.[35–37]

A new important step was made by using Fomblin oil or grease to cover the UCN trap walls [17–20, 38, 39]. It has a pseudo Fermi potential for UCN of $V_0^F = 106$ neV and, being hydrogen free, its loss probability per UCN

wall collision is $\approx 10^{-5}$ at room temperature below the potential threshold.

The precision of neutron lifetime measurements is determined by the accuracy of the estimate of neutron escape rate from the traps, which is the main source of systematic errors.[14, 15, 20, 21, 40] This estimate is based on extrapolation of the measured lifetime τ_1 of neutrons stored in the trap to the zero neutron losses by a careful variation of the bottle geometry and/or temperature so that the wall loss contribution can be accurately determined. The highest precision of τ_n measurements, with the uncertainty of only $\delta\tau_n \sim 1$ s, was announced in large Fomblin-coated material traps [17, 19, 20] and in magneto-gravitational UCN traps[26]. The corresponding neutron lifetime values vary from $\tau_n = 877.7$ s [26] to $\tau_n = 881.5$ s [19, 20]. Such a high precision is achieved by using a large gravitational trap covered with Fomblin grease at low temperature $T < 90$ K to reduce the inelastic neutron scattering. The resulting UCN losses due to the interaction with trap walls were estimated[17, 20] to be $\approx 1/60$ of the neutron β -decay rate. Hence, the corresponding range of extrapolation to account for these losses was only ~ 15 seconds. It is complicated to further notably increase the precision of τ_n measurements without reducing the extrapolation interval. Hence, one needs to reduce the neutron losses due to interaction with the trap walls.

A possible new step to further reduce the neutron escape rate from the trap is to cover the trap walls with liquid ^4He . ^4He does not absorb neutrons at all, but it provides a very small optical potential barrier $V_0^{He} = 18.5$ neV for the neutrons. Hence, only UCN with kinetic energy $E < V_0^{He}$ can be effectively stored in such a trap. The factor $\nu_F \equiv V_0^F/V_0^{He} \approx 5.73$ reduces the neutron phase volume and, hence, the neutron density in the He trap $\nu^{3/2} \approx 13.7$ times as compared to the Fomblin coating. However, the neutron phase-volume density increases with the development of technology[41, 42], and this neutron density reduction factor could become less important than the decrease of neutron loss rate, at least in some experiments.

^4He is superfluid below $T_\lambda = 2.17$ K and covers not only the floor but also the walls and the ceiling of the trap because of the van-der-Waals attraction. On vertical walls the thickness of the helium film depends on the height above the level of liquid helium, as discussed in Sec. III below. On flat vertical walls a few centimeters above the He level and on the ceiling of the trap the thickness of the helium film is expected to be only $d_{He}^{\min} \approx 10\text{nm} < \kappa_0^{-1}$, while the neutron penetration depth into the liquid helium is $\kappa_{0He}^{-1} = \hbar/\sqrt{2m_n V_0^{He}} \approx 33.3$ nm $> d_{He}$. Hence, the corresponding tunneling exponent, approximately giving the reduction of the neutron wave function ψ on the trap wall surface due to its covering by He film,

$$\psi(0)/\psi(d_{He}) \sim \exp(-\kappa_{0He} d_{He}), \quad (1)$$

is of the order of unity: for $d_{He} = d_{He}^{\min} \approx 10\text{nm}$, $\psi(0)/\psi(d_{He}) \approx 0.74$. This is not sufficient to strongly

reduce the neutron losses on the trap walls and to compensate for the decrease of neutron density.

To increase the thickness of He film on the trap walls the idea of neutron storage in a rotating He vessel was proposed[43, 44], but the rotating liquid generates additional bulk and surface excitations. This lead to an enhanced neutron scattering rate, which is very complicated for estimates. Moreover, a moving surface leads to a considerable "upscattering" of neutron, i.e. to gradual increase of their kinetic energy, finally exceeding the potential barrier V_0^{He} . Therefore, one needs a time-independent covering of the trap walls with liquid ^4He .

One can use liquid He to cover only the bottom of neutron trap, where the He film can be made arbitrarily thick. Earth's gravity prevents UCNs from leaving a sufficiently high trap through the upper edge. Neutron escape through the side walls can be reduced by using a very wide trap or by side protection using a magnetic field [45]. However, this partial solution of the problem of small He film thickness does not give a sufficient advantage to use this method in current τ_n measurements.

Liquid He introduces new inelastic scattering mechanism for neutrons because of their interaction with He vapor atoms and with soft thermal excitations - the quanta of surface waves, called riplons. The corresponding scattering rates for a neutron on the lowest vertical level were studied recently.[46] The concentration of ^4He vapor exponentially decreases with temperature, $n_V \propto \exp(-7.17/T [K])$, and can be disregarded below 0.5 K. However, the neutron scattering rate w_R on riplons depends linearly on temperature[46] and, formally, cannot be discarded even below 0.5 K. However, the amplitude of neutron-riplon scattering is small even from the lowest neutron energy level, so that the corresponding scattering time $1/w_R$ exceeds many hours at $T < 0.5$ K.[46] Our preliminary results show that the amplitude of neutron-riplon scattering from higher levels is even smaller. Moreover, the linear temperature dependence of neutron-riplon scattering rate $w_R(T)$ allows its effective extrapolation to zero temperature. Thus, the problem of an additional neutron scattering on a liquid He surface can be solved. However, a small He film thickness remains an obstacle of using liquid He in neutron traps.

In this paper we reanalyze the advantages and drawbacks of covering the UCN trap by helium film. We show that the He film thickness can be effectively increased to become sufficient for the protection of neutrons from losses on trap walls. In Sec. II we calculate the neutron wave function near a flat trap wall covered by liquid He film as a function of neutron energy and of film thickness. This calculation is straightforward and is required to correct the quasiclassical formula (1) and to know what thickness of He film is needed to protect UCN from any notable losses via trap walls. In Sec. III we analyze the profile of He film on a flat vertical trap walls. In Sec. IV we propose a method to increase the He film thickness. In Sec. V we discuss the advantages, drawbacks, and possible prospects

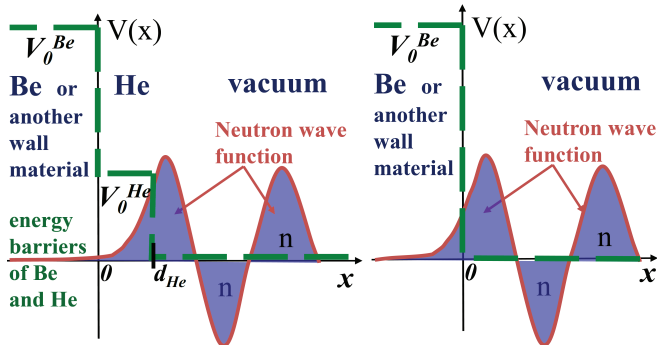


FIG. 1. Schematic representation of the ultracold neutron potential and wave function near the trap wall, covered by He film (a) and without He film (b).

of using liquid helium for improving material traps for the storage of UCN.

II. INFLUENCE OF HELIUM FILM ON THE NEUTRON ABSORPTION RATE INSIDE FLAT TRAP WALLS

In this section we calculate how the neutron wave function decreases inside a flat trap wall covered by liquid He film. We need to determine the minimal He film thickness required to protect the UCN from the absorption inside the wall material. The reader, interested in only the qualitative result of this paper, may skip the straightforward calculations of this section and jump directly to its conclusions, given in Sec. IID. However, for a quantitative study of UCN losses, the results obtained in this section are important. In particular, that (i) the minimal He film thickness required to protect the UCN is $\gtrsim d_{He}^{qm} \approx 100\text{nm}$, and (ii) Eq. (1) ≈ 4 times overestimates the reduction of UCN losses in a wall covered by a helium film of thickness $d_{He} \gtrsim \kappa_{0He}^{-1}$ of our interest.

A. The model

Consider the neutron wave function near the flat wall of a material neutron trap. For an estimate of the influence of He film on neutron absorption rate we study the one-dimensional quantum-mechanical problem, with only one coordinate x . This 1D problem, of course, has been addressed before. In §2.4.3 of the monograph [14] thin films absorbing neutrons were studied. In contrast, here we consider the "insulating" non-absorbing He film and write down explicit relations for the reduction factor of neutron absorption in the material wall due to such a film. Depending on whether the trap wall is covered by He film or not, we have the potential schematically shown in Figs. 1a and 1b. In both cases inside the solid wall at $x < 0$, i.e. in the region I, the neutron wave function is

given by[47]

$$\psi_I(x) = A \exp(\kappa_W x), \quad \kappa_W = \sqrt{2m_n(V_0^W - E)}/\hbar. \quad (2)$$

The neutron absorption rate $1/\tau_a$ inside the material wall for each neutron state, given by its normalized wave function $\psi(x)$, is proportional to the probability w_W of the neutron to be inside the wall, i.e., at $x < 0$:

$$1/\tau_a \propto w_W = \int_{-\infty}^0 dx |\psi(x)|^2 = |A|^2 / \kappa_W. \quad (3)$$

Thus, to estimate the effect of He film on neutron storage time we need to find the normalized neutron wave functions and their coefficients A with and without He film, and to compare the probabilities w_W in Eq. (3). We consider the case when the neutron energy $E = \hbar^2 k^2 / 2m$ is smaller than the helium potential barrier V_0^{He} . Then inside helium at $0 < x < d_{He}$, i.e. in the region II, the neutron wave function

$$\begin{aligned} \psi_{II}(x) &= B_1 \exp(\kappa_{He} x) - B_2 \exp(-\kappa_{He} x) \\ &= B \sinh[\kappa_{He}(x + x_0)], \end{aligned} \quad (4)$$

where

$$\kappa_{He} = \sqrt{2m_n(V_0^{He} - E)}/\hbar = \sqrt{\kappa_{0He}^2 - k^2}. \quad (6)$$

Finally, in vacuum at $x > d_{He}$ the neutron wave function is[47]

$$\psi_{III}(x) = C_1 \exp(ikx) + C_2 \exp(-ikx) = C \sin[k(x + x_1)], \quad (7)$$

where $k \equiv \sqrt{2m_n E}/\hbar$.

B. Wave function amplitudes

Without loss of generality, one can take A to be real. Then, to satisfy the standard boundary conditions (A1) and (A11) at $x = 0$ and at $x = d_{He}$, requiring the continuity of the wave function and its derivative, the coefficients B_1, B_2, B, C, x_0, x_1 must also be real. We assume the trap size $L \gg d_{He}, \kappa_W^{-1}$. Then the normalization of neutron wave function for continuous spectrum, i.e. one particle per unit volume, gives $C = \sqrt{2}$. Applying the boundary conditions to the wave functions (2),(5) and (7), after the straightforward calculations given Appendix A, we obtain the relations between wave-function amplitudes:

$$\begin{aligned} C &= A \sqrt{\kappa_W^2 / \kappa_{He}^2 - 1} \left\{ (\sinh[\kappa_{He}(d_{He} + x_0)])^2 + \right. \\ &\quad \left. + (\cosh[\kappa_{He}(d_{He} + x_0)] \kappa_{He} / k)^2 \right\}^{1/2}, \end{aligned} \quad (8)$$

$$B = A \sqrt{\kappa_W^2 / \kappa_{He}^2 - 1}, \quad (9)$$

and the coordinate shifts

$$x_0 = \frac{1}{2\kappa_{He}} \ln \left(\frac{\kappa_W + \kappa_{He}}{\kappa_W - \kappa_{He}} \right) \approx \frac{1}{\kappa_W}, \quad (10)$$

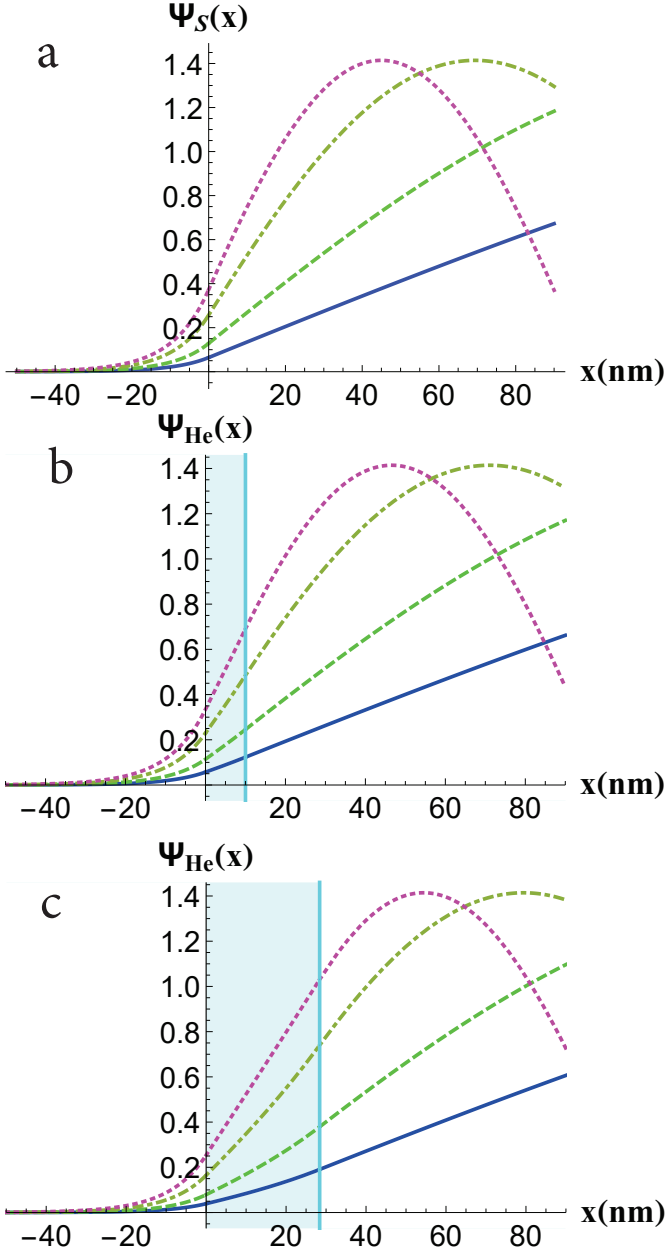


FIG. 2. The neutron wave functions without (a) and with helium film of thickness $d_{He} = 10\text{nm}$ (b) and $d_{He} = 28.5\text{nm}$ (c) at four values of neutron wave vector: $k = 0.005$ (solid blue), 0.01 (dashed green), 0.02 (dot-dashed orange), and 0.03nm^{-1} (dotted magenta).

$$x_1 = \arctan(\tanh[\kappa_{He}(d_{He} + x_0)]k/\kappa_{He})/k - d_{He}. \quad (11)$$

For the "solid" trap wall without helium film, as shown in Fig. 1b, the region II is absent, and we only see the wave functions (2) and (7) at $x = 0$:

$$A_s = C_s \sin[kx_1]; \quad A_s \kappa_W = C_s k \cos[kx_1], \quad (12)$$

which gives

$$C_s = A_s \sqrt{1 + (\kappa_W/k)^2}, \quad (13)$$

$$x_{1s} = \frac{1}{k} \arcsin\left(\frac{1}{\sqrt{1 + (\kappa_W/k)^2}}\right). \quad (14)$$

The neutron wave functions at several k without He film are shown in Fig. 2a, for the minimal He film thickness $d_{He}^{\min} = 10\text{nm}$ at the same k in Fig. 2b, and for He film thickness $d_{He} = 28.5\text{nm}$, corresponding to the height $h = 1\text{cm}$ above He level, in Fig. 2c. These figures illustrate the behavior of neutron wave function $\psi(x)$ near the wall and show that $\psi_I(x)$ inside the wall is strongly suppressed at small neutron momentum k : $\psi(0) \propto 1/k$ at $k \ll \kappa_{He}$. We also see that the thin He film due to Van der Waals attraction to the walls does not change much the neutron wave function.

C. Limiting cases

At small neutron energy $E \ll V_0^{He}$, i.e., $k^2/\kappa_{He}^2 \ll 1$, from Eq. (8) we get

$$C \approx B \kappa_{He} \cosh[\kappa_{He}(d_{He} + x_0)]/k \quad (15)$$

$$= A \sqrt{\kappa_W^2 - \kappa_{He}^2} \cosh[\kappa_{He}(d_{He} + x_0)]/k, \quad (16)$$

and $x_1 \approx x_0$. If we also use $\kappa_W/\kappa_{He} \gg 1$, substituting (10) into (16) we get

$$\begin{aligned} C &\approx \frac{A \kappa_W}{k} \cosh\left[\kappa_{He} d_{He} + \ln \sqrt{\frac{\kappa_W + \kappa_{He}}{\kappa_W - \kappa_{He}}}\right] \\ &\approx \frac{A \kappa_W}{k} \cosh[\kappa_{He} d_{He} + \kappa_{He}/\kappa_W]. \end{aligned} \quad (17)$$

At $E \ll V_0^W$, i.e. at $k/\kappa_W \ll 1$, Eqs. (13) and (14) also simplify:

$$C_s \approx A_s \kappa_W/k; \quad x_{1s} \approx 1/\kappa_W. \quad (18)$$

At $\kappa_{He} d_{He} \ll 1$ and $\kappa_W/\kappa_{He} \gg 1$, Eqs. (17) and (18) coincide. From Eqs. (16) and (17) it follows that the neutron absorption rate $w_W = |A|^2/\kappa_W$ in Eq. (3), both with and without He film, in the limit $k \rightarrow 0$ is strongly suppressed: $w_W \propto k^2 \propto E$. This agrees with the classical picture [15] where the slow neutrons with speed v have (i) longer mean free time $\tau_f \sim L/v$ between hitting the walls, and (ii) spend less time $\tau_t = m_n v/F$ interacting with the wall to reverse their normal velocity due to the force F acting from the wall.

In the opposite limit $E \rightarrow V_0^{He}$, from Eq. (6) we have $\kappa_{He} \rightarrow 0$, $k \rightarrow \kappa_{0He}$, and $k/\kappa_{He} \rightarrow \infty$. This gives

$$x_1 \approx \pi/2k - d_{He}, \quad (19)$$

and from Eqs. (A12) or (8) at $\kappa_{He} d_{He} \ll 1$ and $\kappa_W/\kappa_{He} \gg 1$ we get

$$C \approx A \frac{\kappa_W}{k} \sqrt{1 + k^2(d_{He} + x_0)^2}. \quad (20)$$

At $kd_{He} \ll 1$ this coincides with Eq. (18) without He. However, at $\kappa_{He}^{-1} \gg d_{He} \gtrsim 1/k \approx \kappa_{0He}^{-1}$ the He film reduces the neutron absorption rate $w_W = |A|^2/\kappa_W$ several times, although according to naive formula (1) its effect should be negligible. This makes clear why at $k \rightarrow \kappa_{He}^{-1} \approx 30\mu m^{-1}$ the solid blue and dashed green curves in Fig. 3, corresponding to Eq. (21), are always lower than the dot-dashed magenta curve illustrating Eq. (1).

D. The effect of He film covering the wall on neutron loss

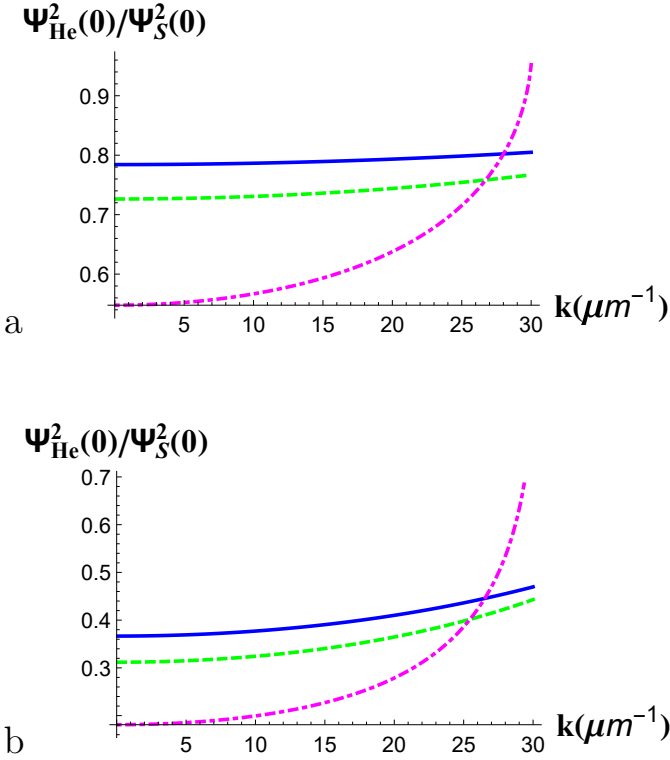


FIG. 3. The reduction factor γ_{He} of neutron losses inside flat trap walls, made of Be (solid blue) and "Fomblin" oil (green dashed), due to the He film of thickness $d_{He} = 10\text{nm}$ (a) and $d_{He} = 28.5\text{nm}$ (b). It illustrates the momentum dependence of γ_{He} given by Eq. (21). For comparison, the dot-dashed magenta curves show $\Psi_{He}^2(0)/\Psi_s^2(0)$ determined using Eq. (1) with κ_{He} given by Eq. (6).

Inside the absorbing wall the neutron wave function is given by Eq. (2) in both cases, with and without He film covering the wall. However, their amplitudes A and A_s differ, and so do the neutron loss rates $1/\tau_a$ given by Eq. (3). Their ratio depends on the neutron energy and on the He film thickness. Combining Eqs. (3), (8) and (13) at $C_s = C$, we obtain the reduction factor γ_{He} of neutron absorption rates $1/\tau_a$ in the trap material due to the He

film:

$$\gamma_{He} = \frac{A^2}{A_s^2} = \frac{1 + (\kappa_W/k)^2}{\kappa_W^2/\kappa_{He}^2 - 1} \left\{ (\sinh[\kappa_{He}(d_{He} + x_0)])^2 + (\cosh[\kappa_{He}(d_{He} + x_0)] \kappa_{He}/k)^2 \right\}^{-1}, \quad (21)$$

where x_0 is given by Eq. (10). The ratio $\gamma_{He} \equiv A^2/A_s^2 = \Psi_{He}^2(0)/\Psi_s^2(0)$ as a function of k for $\kappa_{0W} = \kappa_{0Be}$ and $\kappa_{0W} = \kappa_{0F}$ is shown in Fig. 3. In Fig. 3a we used $d_{He} = 10\text{nm}$, corresponding to the minimal He film thickness. One sees that this ratio is close to unity, which means that the effect from a very thin He film due to the additional suppression of the neutron wave function is not very important for neutron loss rate. However, in Fig. 3b we show A^2/A_s^2 for the same set of k but at $d_{He} = 28.4\text{nm}$, corresponding to the He film thickness at height $h = 1\text{cm}$. The effect of He film at $d_{He} = 28.4\text{nm}$ is already considerable, as it reduces the neutron absorption rate ≈ 3 times.

In the limit $k^2 \ll \kappa_{He}^2$ Eq. (21) simplifies to

$$\frac{A^2}{A_s^2} = \cosh^{-2} \left[\kappa_{He} d_{He} + \frac{1}{2} \ln \sqrt{\frac{\kappa_W + \kappa_{He}}{\kappa_W - \kappa_{He}}} \right] / \left(1 - \frac{\kappa_{He}^2}{\kappa_W^2} \right). \quad (22)$$

This absorption-rate ratio is independent of k , because both A^2 and $A_s^2 \propto k^2$. Comparing Eqs. (22) and (1) we obtain that the latter gives the absorption rate $1/\tau_a$ smaller than the correct result by a factor of 4 at $\kappa_{He} d_{He} \gg 1$ and $k \ll \kappa_{He} \ll \kappa_W$, which is also seen from Fig. 4.

The dependence of $\gamma_{He} \equiv A^2/A_s^2$ on the film thickness d_{He} at several k is shown in Fig. 4 for a beryllium wall. For the trap walls covered by "Fomblin" oil the dependence A^2/A_s^2 on d_{He} looks very similar to Fig. 4 and, hence, is not shown here. For convenience the plot is given in logarithmic scale. One sees that the expected exponential suppression (1) of neutron probability density inside liquid helium starts from film thickness $\approx 20\text{nm}$. For comparison, by thin solid lines of the same colors in Fig. 4 we also show the predictions of Eq. (1), which are quantitatively incorrect. At small k Eq. (1) gives a neutron absorption rate ≈ 4 times smaller than the exact result (21). At large $k \rightarrow \kappa_{0He}$, in contrast, Eq. (1) predicts a too large absorption rate, as follows from Eq. (20) and discussed after it.

The simple calculations of this section show several points, important for possible application of He films to reduce neutron losses inside a material trap. First, the approximate estimate in Eq. (1) works qualitatively but not quantitatively. At low neutron energy $E < 0.7V_0^{He}$, which is of main interest, the calculated γ_{He} in Eq. (21) is up to four times smaller than γ_{He} predicted from Eq. (1), as follows from Eq. (22) and is shown in Figs. 3 and 4. As illustrated in Fig. 4, this discrepancy increases with film thickness and reaches four times at $d_{He} \gg \kappa_{He}^{-1}$. At large energy $E \rightarrow V_0^{He}$, on contrary, Eq. (1) predicts too small reduction factor γ_{He} , as follows from Eq. (20). Especially, this is clear at $E \geq V_0^{He}$, where according to Eq. (1) $\gamma_{He} = 1$, because the imaginary part of neutron

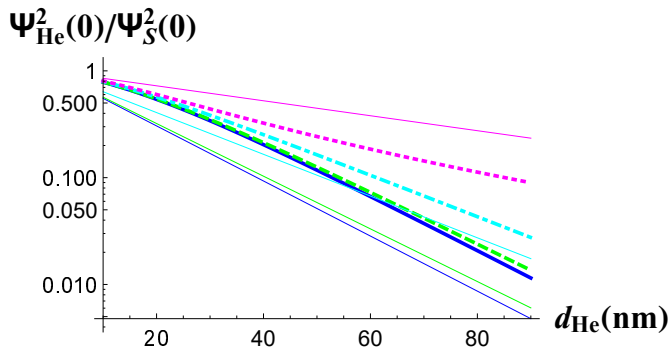


FIG. 4. The squared ratio (in logarithmic scale) of neutron wave functions on the wall surface, made of Be, as a function of helium film thickness d_{He} at four different values of neutron wave vector $k = 0.005$ (solid blue), 0.01 (dashed green), 0.02 (dot-dashed cyan), and 0.03nm^{-1} (dotted magenta). Thin solid curves of the corresponding colors show the predictions of Eq. (1).

momentum is zero. This discrepancy at $E \gtrsim V_0^{He}$ appears because Eq. (1) neglects the backscattering of neutron waves from the He surface, which takes place even if $E > V_0^{He}$.

The second, physical conclusion from the above calculations is that a thin He film of thickness $10 - 30\text{nm}$, formed only by the Van der Waals attraction of superfluid helium to the trap walls, is not sufficient to completely avoid the neutron losses due to the absorption inside the wall material. The neutron absorption rate $1/\tau_a$ inside an ideal flat wall reduces due to such a thin He film only by a factor $\gamma_{He} \equiv A^2/A_s^2 \sim 0.3 - 0.8$ (see Figs. 3 and 4), depending on the film thickness determined by the height h above He level (see next section). As one sees from Fig. 4, to reduce a hundred times the neutron losses due to the absorption in material walls by covering with liquid helium, the He film thickness must be $d_{He} \gtrsim d_{He}^{qim} = 100\text{nm}$.

III. HELIUM FILM PROFILE ON A FLAT VERTICAL WALL

The study of the profile of superfluid helium film on vertical walls, i.e. the dependence of He film thickness d_{He} on the height z above liquid helium level, turned out to be a non-trivial problem, both experimentally[48–53] and theoretically[51–54].

According to classical fluid mechanics,[55] the meniscus profile is given by

$$\frac{d_{He}(h)}{a_{He}} = \text{arccosh}\left(\frac{2a_{He}}{h}\right) - \text{arccosh}\left(\frac{2a_{He}}{h_0}\right) - \sqrt{4 - h^2/a_{He}^2} + \sqrt{4 - h_0^2/a_{He}^2}, \quad (23)$$

where the capillary length of liquid ${}^4\text{He}$ is $a_{He} = \sqrt{\sigma_{He}/g\rho_{He}} = 0.5\text{mm}$ and $h_0 = \sqrt{2a_{He}}\sqrt{1 - \sin\theta}$ is the

maximal height to which the fluid rises at the wall. Here $\sigma_{He} = 0.354\text{dyn/cm}$ is the surface tension coefficient of liquid ${}^4\text{He}$, $g = 9.8\text{m/s}^2$, and $\rho_{He} \approx 0.145\text{g/cm}^3$. Even for the zero contact angle θ , according to Eq. (23), the film thickness $d_{He} = 0$ for $h > h_0$. This is not the case for superfluid helium that covers the walls and ceiling of the trap by a thin film of thickness $d_{He}^{\text{min}} \approx 10\text{nm}$ at arbitrary height h because of the Van der Waals attraction to the walls. However, the correct profile of helium film is not just the sum of $d_{He}(h)$ in Eq. (23) and the minimal film thickness $d_{He}^{\text{min}} \approx 10\text{nm}$.

The simple theory of the superfluid He film profile at $h > h_0$ assumes that the total energy E_{tot} of a ${}^4\text{He}$ atom on the surface of He film in equilibrium does not depend on the height h . This total energy contains the gravitational energy $M_{He}gh$ of this atom and its Van der Waals attraction V_W to the wall. As a result, one obtains an equation relating d_{He} and h :

$$E_{tot}(h) = M_{He}gh + V_W(d_{He}) = 0. \quad (24)$$

The Van der Waals attraction to other He atoms is assumed to be the same on the surface of thin He film on the wall and on the thick film covering the vessel bottom. Therefore, it is omitted in Eq. (24). The microscopic theory giving

$$V_W(d_{He}) \propto d_{He}^{-n} \quad (25)$$

was developed in Ref. [54], where $n = 3$ or 4 depending on the distance and wall material. Combining Eqs. (24) and (25) gives

$$d_{He}(h) = d_0/h^{1/n}. \quad (26)$$

The experiments[48–53] confirmed Eq. (26), but the values of d_0 and of the exponent $1/n$ slightly vary depending on the measurement method. If one denotes $d_0 \equiv d_{He}(h = 1\text{cm})$, and the height h is also given in units of cm, the latest measurement[53] using the He oscillation method suggests $d_0 = 28.5\text{nm}$ and $1/n \approx 1/3.5 = 0.286$. This reasonably agrees with earlier measurements using He oscillations[48] and optical methods[49, 56]. The latter suggests[56] slightly different values $d_0 = 30\text{nm}$ and $n \approx 2 - 3$. At smaller h the exponent increases[50, 51] to $1/n \approx 0.5$. For example, measurements using the microbalance weight method at $h > 3\text{mm}$ at temperature $1.2\text{K} < T < 2.13\text{K}$ suggest[50] much thicker film and the parameters $d_0 \approx 118\text{nm}$ and $n \approx 2$. The functions $d_{He}(h)$ from Eqs. (23) and (26) are plotted in Fig. in logarithmic scale. As one sees from this plot, the sewing of Eqs. (23) and (26) is still lacking, because, unfortunately, we could not find data on $d_{He}(h)$ in the region $h_0 < h < 3\text{mm}$, while Eq. (23) is not valid there. Probably, in this region the exponent in Eq. (26) further increases to $1/n > 0.5$. Figure 5 shows the general dependence $d_{He}(h)$ and can be used for the estimates of neutron absorption rate on a flat vertical wall covered by superfluid helium.

Although the He meniscus is wide enough to completely protect neutrons from absorption inside a solid wall material, according to Eq. (21), its height is too small.

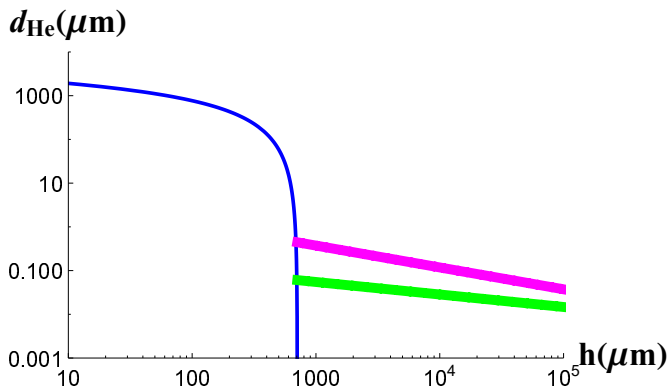


FIG. 5. The functions $d_{He}(h)$ from Eq. (23) (solid blue curve) and from Eq. (26) with the parameters[53] $d_0 = 28.5nm$ and $1/n \approx 1/3.5$ (dashed green line) and[50] $d_0 = 118nm$ and $1/n \approx 0.5$ (dash-dotted magenta line).

Neutrons with energy $E = E_{\max} = V_0^{He} = 18.5neV$ in the earth's gravity potential may reach the height $h_{\max} = E/m_n g \approx 18cm$. The meniscus height is only $h_m \approx 0.7mm$, i.e., much smaller. Hence, most neutrons with energy $E < V_0^{He}$ heat the trap walls much higher than He meniscus, where the thickness of He film covering an ideal flat vertical wall is only determined by the Van der Waals forces.

IV. HE FILM ON A ROUGH WALL

The wall roughness, usually, enhances 2-3 times the neutron losses due to the absorption inside trap walls.[14, 15] This happens because the wall roughness makes the repulsion potential of the walls smoother, so that the neutron wave function penetrates deeper into the walls.[14, 15] However, the wall roughness may considerably increase the average He film thickness due to capillary effects, thus reducing the neutron losses. Indeed, the wall roughness increases its surface area, raising the role of capillary effects. If the length scale of surface roughness $l_R \ll a_{He}$, to minimize the surface tension energy the He film even on a rough wall must have almost flat interface with vacuum. Hence, the superfluid helium fills all small cavities of size $l_R \lesssim a_{He}$ in the wall.

To describe the He profile one has to minimize the energy functional of He film,

$$E_{tot} = V_g + E_s + V_W, \quad (27)$$

instead of considering a single He atom, as we did in Eq. (24). Here the gravity term is

$$V_g = \rho_{He} g \int z d_{He}(\mathbf{r}_{||}) d^2 \mathbf{r}_{||}, \quad (28)$$

where $\mathbf{r}_{||} = \{y, z\}$ is a 2D coordinate vector along the wall plane, y and z are the horizontal and vertical coordinates along the wall,

$$d_{He}(\mathbf{r}_{||}) = \xi(\mathbf{r}_{||}) - \xi_W(\mathbf{r}_{||}) \quad (29)$$

is the coordinate dependent He film thickness, and the functions $\xi(\mathbf{r}_{||})$ and $\xi_W(\mathbf{r}_{||})$ describe the surface profiles of He and of trap wall. Below we consider a wall roughness with typical length scale $\lesssim a_{He} \ll h_{\max}$. The variation of the coordinate z on this small length scale can be neglected compared to its average $\langle z \rangle$, i.e., its height $h = \langle z \rangle$ above the He level. Hence, in Eq. (28) the coordinate z can be replaced by the height h of the wall roughness.

The second term in Eq. (27), describing the surface tension energy, is given by

$$E_s = \sigma_{He} \int \sqrt{1 + [\nabla \xi(\mathbf{r}_{||})]^2} d^2 \mathbf{r}_{||}. \quad (30)$$

Its square-root dependence complicates the problem of finding an exact surface profile $\xi(\mathbf{r}_{||})$. Usually, its analytical solution is available only in the limit $|\nabla \xi(\mathbf{r}_{||})| \ll 1$.

The gravity and surface tension, i.e., the first two terms in Eq. (24), are important on a macroscopic length scale $\gtrsim a_{He}$. The last van der Waals term V_W , describing the helium attraction to the wall material, acts on a much shorter distance $\lesssim d_{He}^{\min} \approx 10nm \ll a_{He}$. We have a very lucky situation for a theoretical analysis, because the van der Waals length scale $\sim d_{He}^{\min}$ is five orders of magnitude smaller than the capillary length scale a_{He} . Hence, the influence of gravity and of the surface tension of free He surface on V_W can be neglected. For a flat wall surface the van der Waals term V_W depends only on the wall material and on the film thickness: $V_W = V_W(d_{He})$. Without surface tension it would lead to the covering of a rough surface by a He film of thickness $d_{He} \sim d_{He}^{\min}$, which almost repeats the wall profile if $l_R \gg d_{He}^{\min}$. Thus one may keep only two first terms in the functional $E_{tot}[\xi(\mathbf{r}_{||})]$ in Eq. (27), reducing the effect of van-der-Waals term V_W to the "boundary conditions" of the minimal He film of thickness $d_{He} \sim d_{He}^{\min}$.

Such a minimal He film of thickness $d_{He} \sim d_{He}^{\min}$, caused by the van der Waals attraction, would cost an additional surface tension energy ΔE_s , which may be larger than the gravity term ΔV_g of extra helium needed to make the He surface even flat: $\xi(\mathbf{r}_{||}) = const = \max\{\xi_W(\mathbf{r}_{||})\} + d_{He}^{\min}$. This additional amount of helium depends on the wall profile and may strongly increase the average thickness of He films. Below we consider several types of surface roughness. We do not calculate exact surface profiles $\xi(\mathbf{r}_{||})$ for particular functions $\xi_W(\mathbf{r}_{||})$, but make some simple qualitative estimates of the roughness parameters when the surface tension leads to almost flat He surface $\xi(\mathbf{r}_{||})$.

A. Hemispherical cavity

Consider a semispherical cavity of radius R , $d_{He}^{\min} \ll R \lesssim a_{He}$, located in a wall at a height h above the liquid He level. Due to the van der Waals forces, its surface is covered by superfluid helium film. However, due to capillary effects, for small $R \lesssim a_{He}^2/h$ this cavity is almost totally filled with helium. Indeed, a thin He film of thickness

d_{He} on the surface of a hemisphere has the total surface $S = 2\pi(R - d_{He})^2 \approx 2\pi R^2$, and the corresponding surface tension energy loss is $E_{s1} \approx 2\pi R^2 \sigma_{He}$. If this cavity is totally filled with He, this surface tension energy reduces to $E_{s2} \approx \pi R^2 \sigma_{He}$, but the gravitational energy increases by $E_g \approx 2\pi R^3 \rho_{He} g h / 3$. Hence, it is energetically favorable to fill the cavity by helium if $E_g < \Delta E_s \equiv E_{s1} - E_{s2}$, or if

$$R < R_0(h) \approx 3\sigma_{He}/2\rho_{He}gh = 3a_{He}^2/2h. \quad (31)$$

For $h = h_{\max} = 18\text{cm}$, this gives $R_0 \approx 2\mu\text{m}$. Helium film of such thickness is more than enough to protect neutrons from absorbing inside the material wall. Of course, the exact He surface profile inside a hemispherical cavity is not spherical or flat, and even for $R > R_0(h)$ the cavity will be partially filled with liquid helium, so that the film thickness $d_{He} \gg \kappa_{He}^{-1}$. An additional and important advantage of He film on the walls is that it fills the surface cavities, thus reducing the neutron losses caused by surface roughness.

The above simple estimate demonstrates the possibility of a strong increase of the effective thickness of He film on the trap walls. The natural surface roughness depends on materials and their preparation, which is a subject of much investigation [57]. We propose to create the special roughness of trap walls to increase the effective thickness of He film and, hence, to reduce the neutron losses.

B. Ribbed wall surface

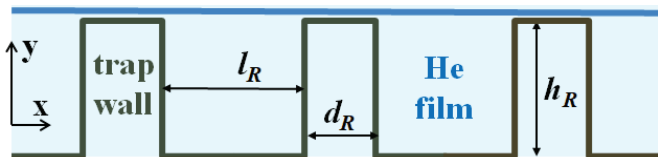


FIG. 6. The steplike roughness of the wall surface covered by liquid helium with an almost flat surface.

Now consider a periodic 1D roughness of an asymmetric square-wave form, i.e., of straight rectangular protrusions (ridges) as shown in Fig. 6. Again we compare the energies of two He configurations: (i) thin He film covering the wall surface due to van der Waals term V_W and (ii) flat surface completely covering the surface roughness. The estimates are similar to those in the previous subsection. The gravity energy per unit length is $E_g \approx \rho_{He} g h h_R l_R$, where h is again the height on the wall, h_R is the roughness height, and l_R is the distance between the ridges. The surface energy difference for these two configurations per unit length is $\Delta E_s \approx h_R \sigma_{He}$. It is energetically favorable to fill the roughness by helium if $\Delta E_s > E_g$, or if

$$l_R < l_0(h) \approx \sigma_{He}/\rho_{He}gh = a_{He}^2/h. \quad (32)$$

The roughness height h_R can be made larger than $d_{He}^{aim} = 100\text{nm}$. Then the only neutron absorption in the wall

material is due to the rectangular protrusions. However, the volume part ϕ of such protrusions is small, $\phi \approx d_R/l_R \ll 1$, where d_R is the ridge width (see Fig. 6). Using Eq. (32) we obtain the minimal value of this volume fraction, $\phi_{\min} \approx d_R h / a_{He}^2$. If one takes the width of ridges $d_R \approx 0.1 d_{He}^{aim} = 10\text{nm}$, which is sufficient for the full van der Waals attraction of He to the wall, and $h = h_{\max} = 18\text{cm}$, one obtains $\phi_{\min} \approx d_R h_{\max} / a_{He}^2 = 7.2 \times 10^{-3}$, i.e., more than a hundred times reduction of neutron losses due to the absorption inside wall material.

Making the height of protrusions on the wall ten times higher than their width looks technically difficult because of their fragility. To raise the durability of surface roughness, one may use zig-zag instead of straight grooves. Taking thicker ridges with $d_R \approx d_{He}^{aim} = 100\text{nm}$ gives $\phi_{\min} \approx 0.07$ and the neutron loss reduction factor $\gamma \approx 1/14$. This is also good. To further increase the efficiency of He film protection one may consider other roughness configurations. One possibility is to make height-dependent linear density of ridges $1/l_R \propto h$. According to Eq. (32), $1/l_R > 1/R_0(h) = h/a_{He}^2$. Making $1/l_R = h/a_{He}^2$ instead of $1/l_R = h_{\max}/a_{He}^2$ reduces the protrusion density twice, thus diminishing the neutron losses due to the wall absorption by a factor ≈ 28 .

Note that the required small period $l_R = a_{He}^2/h_{\max} \approx 1.4\mu\text{m}$ of surface roughness is technically achievable by many methods. Diffraction gratings of this and even smaller periods are commercially available. Even a much shorter period $l_R \leq 100\text{nm}$ of the grating is technically possible with a rather high precision by using electron-beam lithography.[58] The coverage of UCN trap walls by the powder of diamond nanoparticles, often used in experiments with UCN [59], may also create the required surface roughness to make the helium film sufficiently thick.

C. Fur surface roughness

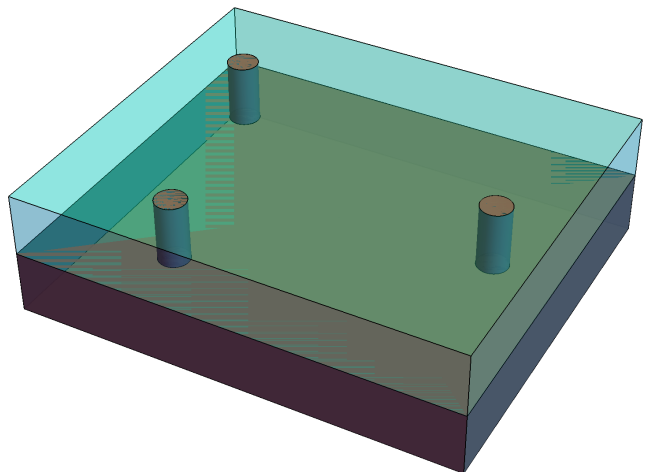


FIG. 7. Schematic view of a furry rough wall surface covered by liquid helium.

Another way to optimize the surface roughness is to make it "furry". This type of disorder on neutron trap walls was much investigated theoretically [14, 15], because it corresponds to a random surface roughness with short-range Gaussian correlation function. We approximate this roughness by randomly situated thin cylinders of height h_R , diameter $d_R \gg d_{He}^{\min}$, and surface density n_R , protruding from the flat trap wall, as shown in Fig. 7. Each cylinder increases the surface area by $\Delta S \approx \pi d_R h_R$, and covering the fur with He film reduces the surface tension energy by $\Delta E_s \approx \pi d_R h_R \sigma_{He} n_R$. The gravitational energy of such a He film per unit wall area is $E_g \approx \rho_{He} g h h_R$. It is energetically favorable to fill the "fur" roughness by liquid helium if $\Delta E_s > E_g$, or if the fur density

$$n_R > n_R(h) = h/\pi d_R a_{He}^2. \quad (33)$$

Taking this fur density $n_R(h) = h/\pi d_R a_{He}^2$, one obtains the volume fraction ϕ of such protrusions in the He film to be

$$\phi = \int_0^{h_{\max}} (\pi d_R^2/4) n_R(h) dh/h_{\max} = d_R h_{\max}/8 a_{He}^2. \quad (34)$$

Taking the cylinder diameter equal to its height, $d_R = h_R \approx d_{He}^{\text{aim}} = 0.1 \mu m$, one obtains that the neutron losses due to the wall absorption can be reduced by a factor $\gamma = 1/\phi \approx 110$. Even a much lower surface roughness, when the cylinder height is equal to only 1/10 of its diameter, reduces the neutron losses by a factor > 10 . Taking into account another benefit from using He film, namely, the elimination of negative effect of surface roughness on neutron losses, this shows a strong advantage of using superfluid He to cover the walls of a neutron trap.

Before ending this section we note that the surface roughness and the corresponding increase of the effective He film thickness due to capillary effects may explain the discrepancy of experimental values determined by different methods [48–53]. Indeed, the microbalance weight method [50] measures the total He weight. This He weight includes the filled cavities on the surface, which are not detected by optical methods [49, 56]. Hence, the weight method gives a thicker He film on a rough surface [50]. Since the typical He film thickness due to van der Waals forces is small, $d_{He} \sim 10 \text{nm}$, even a tiny surface roughness of height $\sim 10 \text{nm}$ may strongly affect the measured values of He film.

V. DISCUSSION

^4He does not absorb neutrons and can be used to protect neutrons from the absorption inside the material of trap walls, thus considerably increasing the neutron storage time. However, liquid He introduces new scatterer for neutrons: the He vapor atoms and the soft thermal excitations - the quanta of surface waves, called ripples. Let us summarize the benefits and disadvantages of covering the UCN trap walls with liquid helium.

I. Drawbacks.

1. Liquid ^4He has a very small optical potential barrier $V_0^{He} = 18.5 \text{neV}$ for the neutrons, which is about one order of magnitude smaller than most of other materials used for UCN solid traps. Hence, only UCN with kinetic energy $E < V_0^{He}$ can be effectively stored in such a trap. Hence, the corresponding UCN density inside a He trap is about one order of magnitude smaller than inside traps made of other materials. Unfortunately, the only way to overcome this drawback is to increase the neutron density coming from their source. The simple neutron manipulations using any external potential cannot increase the density of neutrons with energy $E < V_0^{He}$ because of the Liouville's theorem, stating the conservation of particle density in phase space for Hamiltonian systems. However, modern neutron reactors give rather high neutron intensity.[60] Hence, the reduction of UCN density in a trap by an order of magnitude is important but not crucial. More complicated neutron manipulations, e.g., using inelastic magnetic scattering in weakly absorbing cold paramagnetic systems [42], probably, may further increase the density of UCN.

2. A thick He film covers only the bottom of the neutron trap. Due to capillary effects, the flat vertical walls on the height $h < a_H \sqrt{2} \approx 0.7 \text{mm}$ is also covered by liquid helium of sufficient thickness $d_{He} \sim a_H$. However, the maximal height h_{\max} to which the UCN with kinetic energy $E < V_0^{He}$ may fly is much larger than $a_H \sqrt{2}$: $h_{\max} \approx 18 \text{cm}$. Above the height $a_H \sqrt{2}$ the superfluid He covers the flat walls due to the van der Waals attraction, but the corresponding He film thickness $d_{He} = 10 - 30 \text{nm}$ is not sufficient to protect the neutrons from their penetration into the wall material. One needs a thicker He film $d_{He} > d_{He}^{\text{aim}} \approx 100 \text{nm}$ at a height $h < h_{\max}$ to make an effective protection. Luckily, this drawback can be overcome. In Sec. III we propose a method to increase the thickness of He film by using the surface roughness. Our estimates in Sec. III show the feasibility of a strong reduction of UCN losses due to the absorption inside trap walls.

3. Liquid He introduces new scattering mechanisms of UCN: the He vapor atoms and the soft thermal excitations - the quanta of surface waves, called ripples. The corresponding scattering rates were recently calculated for a neutron on the lowest vertical level [46], and these estimates are qualitatively valid for higher levels. The energy of ^4He evaporation is 7.17K per atom. Hence, the concentration of vapor exponentially decreases with temperature, $n_V \propto \exp(-7.17/T [K])$. The scattering on He vapor can be disregarded at low $T < 0.5K$. However, such a low temperature is very essential; at twice higher $T = 1K$ the neutron lifetime due to scattering rate on He vapor is only 2.3 min. The ripples, the quanta of surface waves, are gapless excitations with soft spectrum: $\omega_q^2 = (\sigma_{He}/\rho_{He}) (q^2 + a_H^{-2}) q$. The neutron scattering rate w_R on ripples depends linearly on temperature [46] and, formally, cannot be discarded even below 0.5K. Luckily, the amplitude of neutron-ripple interaction is small, and

the corresponding neutron scattering time $1/w_R$ exceeds many hours at $T < 0.5K$. Moreover, the linear temperature dependence of neutron-ripplon scattering rate $w_R(T)$ allows it to be effectively taken into account by extrapolation to zero temperature. Nevertheless, to avoid new scattering mechanisms of UCN, introduced by helium, low temperature $T < 0.5K$ is required.

4. The liquid ^4He covering the trap walls must be isotopically pure, because ^3He absorbs neutrons. The ^4He isotope purification technology was developed long ago [61–63]. The superfluid heat flush method allows reducing the ^3He concentration to less than 5×10^{-13} [62], which is sufficient to neglect the UCN losses due to the absorption by ^3He . Note, that this degree of isotopic purification is achieved even in a continuous flow apparatus at a production rate of $3.3 \text{ m}^3\text{h}^{-1}$ at STP [62].

II. Advantages.

1. For large neutron traps of size $L \gg h_{\text{max}}$ the most important neutron losses are due to their collisions with the trap bottom. This is clear by just comparing the corresponding surface areas: their ratio is $\sim h_{\text{max}}/L$. Liquid He covers the trap bottom as a thick film, sufficient for complete protection of neutrons with energy $E < V_0^{\text{He}}$ from being absorbed inside the trap material.

2. As shown in Sec. III, due to the combination of capillary effects with the van der Waals attraction, the surface roughness of trap walls strongly increases the effective He film thickness on them. For various roughness configurations, e.g., as discussed in Sec. III, one can easily achieve He film thickness on the walls to be sufficient for almost complete UCN protection from absorption inside trap material. This may strongly, by 1-2 orders of magnitude, diminish the neutron losses inside material traps.

3. Superfluid He fills cavities and other surface roughness, thus removing their negative effect on the neutron storage time in material traps. The negative effect of surface roughness without He was estimated to increase 2-3 times the neutron losses from wall absorption[15]. Eliminating this negative effect is a considerable advantage, which also leads to longer UCN storage times.

The above list and discussion of weak and strong points of liquid He film covering UCN traps shows that the potential advantage is much stronger than the drawbacks. A possible experiment may use similar methods as in current UCN τ_n measurements with walls covered by Fomblin oil [17, 20]. Such an experiment contains five stages [17, 20]: (1) filling, (2) monitoring (with spectrum preparation), (3) holding, (4) emptying, and (5) measurement of background. Helium film may prevent the filling of a UCN trap with neutrons using standard valves in the trap bottom, but the neutrons can be filled from the top either (1) with the help of an additional time-dependent potential created by a magnetic field, or (2) by moving up and/or rotating the trap itself, as in Refs. [17, 20]. Since the gravitational potential difference is only 100 neV/m, and the magnetic field creates a potential 60 neV/T, a small vertical magnetic-field gradient 16mT/cm compensates for the rise of UCN kinetic energy when they are filled from

the top of the trap for half of UCN with one spin projection. A specially designed time-dependent magnetic field may even decelerate and move the neutrons [64], of course, conserving their phase-space density according to the Liouville's theorem.

The accuracy of proposed τ_n measurements using such UCN traps covered by liquid helium is limited by (1) the statistical error, (2) uncertainties in the rate of inelastic neutron scattering by excitations of liquid helium, and (3) the remaining UCN absorption in the trap wall material, if some part of the wall is covered by too thin He film. The statistical error depends very much on the experimental setup and procedure. It can be reduced only by increasing the UCN density in the holding stage or by performing several cycles/replicas of τ_n measurement. The inelastic scattering rate $1/\tau_i$ of UCN by surface and bulk excitations in liquid helium was estimated [46] to be rather small at $T < 0.5K$, when the concentration of He vapor is exponentially small. The main contribution to UCN scattering rate at $T < 0.5K$ comes from ripples – the quanta of surface waves. For a neutron on the lowest vertical quantum level but with large in-plane neutron energy $K = 100\text{neV}$, the rate $1/\tau_r$ of its scattering to continuous spectrum via ripplon absorption was roughly upper estimated [46] to be less than $1/\tau_r^{up} \approx 2 \times 10^{-5}\text{s}^{-1} \times T[\text{K}]$ (see Eq. (D17) of Ref. [46]). However, the UCN scattering rate in our problem is considerably less than the above estimate $1/\tau_r^{up}$ for several reasons. The first and, probably, most important difference between our case and the one in Ref. [46] is that in Ref. [46] the neutron was on the lowest energy level in the vertical direction. Hence, the typical value $\psi_{\perp}(0)$ of its normalized wave function on the helium surface $z = 0$ was rather large, because this wave function extends to only a distance $L_{\psi} \sim 10\mu\text{m}$ from the surface. In our case the neutron wave function is localized on a distance $L_{\psi} \leq h_{\text{max}} = 18\text{cm}$ above the He surface, which is 10^4 times larger. Hence, the normalization coefficient of this wave function, entering $\psi_{\perp}(0)$, is 100 times smaller. Since the UCN scattering rate by ripples is $1/\tau_r \propto |\psi_{\perp}(0)|^2$, this may reduce by orders of magnitude the rate of ripplon absorption by UCN with typical out-of-plane component of kinetic energy $E_{\perp} \sim V_0^{\text{He}}/5$. Second, the in-plane neutron velocity $v_{||}$ in our problem is much smaller than in Ref. [46] and does not exceed $v_{||\text{max}} = \sqrt{2V_0^{\text{He}}/m} = 1.9\text{m/s}$. Since the scattering rate τ_r^{-1} increases with the increase of $v_{||\text{max}}$, this factor also reduces τ_r^{-1} in our case. Third, the calculations in Ref. [46] are too rough, because they are aimed to show that τ_r^{-1} is negligibly small for a different experiment. Our current preliminary estimates even for the lowest vertical neutron level, i.e., neglecting the first factor above, give that $1/\tau_r < 10^{-5}\text{s}^{-1} \times T[\text{K}]$. At $T = 0.5K$ this τ_r^{up} corresponds to UCN loss probability $< 0.4\%$ of β -decay probability, which is already much better than in the most precise UCN τ_n measurements and can be easily accounted for using the temperature extrapolation of measured $\tau_n(T)$ to $T = 0$ due to its linear T -dependence. Note that the predicted $\tau_r^{-1}(T) \propto T$ with very high precision, because

the typical riplons, important for UCN scattering, have energy $\hbar\omega_r \sim V_0^{He} \ll T$, hence, their equilibrium density $\propto T$. The problem of inelastic UCN scattering is also important in current τ_n measurements using Fomblin oil [17–20, 38, 39]. Even with a nonlinear temperature dependence of inelastic scattering rate in these experiments the standard temperature extrapolation allows reducing the systematic error due to inelastic neutron scattering by an order of magnitude. The linear temperature dependence of the ripplon absorption rate τ_r^{-1} allows it to be accounted for with much higher precision by similar temperature extrapolation of measured $\tau_n(T)$ to $T = 0$. Thus, if helium temperature is reduced to $T = 0.2\text{K}$, the expected systematic error of UCN τ_n value due to ripplon scattering is less than 0.01%. More accurate calculations of the UCN scattering rate by riplons, similar to those in Ref. [46] but taking the velocity distribution of UCN in our particular problem, most probably, will further reduce the estimate of UCN scattering rate by riplons. The last important factor, affecting the accuracy of τ_n measurements, is the remaining UCN absorption in the trap wall material, if some parts of the wall are covered by too thin He film. Although this error is greatly reduced by using liquid He, it may still be present due to any local distortions of wall roughness. This type of errors can be effectively taken into account by the standard size extrapolation method, similar to that in Refs. [17, 20, 38], which makes the corresponding systematic error negligibly small in our case.

To summarize, liquid He film may reduce a hundred times the neutron absorption rate inside UCN trap material. This superfluid He film can be made thicker than the neutron penetration depth due to capillary effects by using a rough wall surface. This has a potential to strongly improve the accuracy of neutron lifetime measurements and of other experiments with UCN, important for particle physics, astrophysics, and cosmology. It may also help to explain the discrepancy between measured neutron β -decay times using cold neutron beams and UCN magnetic and material traps.

ACKNOWLEDGMENTS

P.G. acknowledges the support of the Ministry of Science and Higher Education of the Russian Federation in the framework of Increase Competitiveness Program of NUST "MISIS" Grant No. K2-2020-038. A.D. acknowledges the State Assignment No. 0033-2019-0001.

Appendix A: Calculation of the neutron wave function near the He-covered trap wall

First consider the trap wall covered by helium film, as shown in Fig. 1a.

1. Sewing of wave functions at $x = 0$

The boundary conditions on the neutron wave function at $x = 0$ are written as[47]

$$\psi(-0) = \psi(+0), \quad \psi'(-0) = \psi'(+0). \quad (\text{A1})$$

Substituting the wave functions (2) and (5) to Eq. (A1) gives

$$A = B_1 - B_2, \quad A\kappa_W = \kappa_{He}(B_1 + B_2), \quad (\text{A2})$$

or

$$B_2 = B_1 \frac{\kappa_W - \kappa_{He}}{\kappa_W + \kappa_{He}}, \quad A = \frac{B_1 2\kappa_{He}}{\kappa_W + \kappa_{He}}. \quad (\text{A3})$$

These relations can be rewritten as

$$B_1 = A \frac{\kappa_W + \kappa_{He}}{2\kappa_{He}}, \quad B_2 = A \frac{\kappa_W - \kappa_{He}}{2\kappa_{He}}. \quad (\text{A4})$$

Let us relate the coefficients B_1 , B_2 , and B in Eq. (5). Since

$$\psi_{II}(x) = B \sinh(\kappa_{He}[x + x_0]) = \quad (\text{A5})$$

$$= \frac{B}{2} \exp(\kappa_{He}[x + x_0]) - \frac{B}{2} \exp(-\kappa_{He}[x + x_0]), \quad (\text{A6})$$

we obtain

$$B_1 = \frac{B}{2} \exp(\kappa_{He}x_0), \quad B_2 = \frac{B}{2} \exp(-\kappa_{He}x_0), \quad (\text{A7})$$

and

$$B = 2\sqrt{B_1 B_2} = 2B_1 \sqrt{\frac{\kappa_W - \kappa_{He}}{\kappa_W + \kappa_{He}}} = A \sqrt{\frac{\kappa_W^2}{\kappa_{He}^2} - 1}. \quad (\text{A8})$$

The coordinate shift

$$x_0 = \frac{1}{2\kappa_{He}} \ln\left(\frac{B_1}{B_2}\right) = \frac{1}{2\kappa_{He}} \ln\left(\frac{\kappa_W + \kappa_{He}}{\kappa_W - \kappa_{He}}\right). \quad (\text{A9})$$

Usually, $\kappa_{He}/\kappa_W < \kappa_{0He}/\kappa_{0W} \ll 1$; if the wall material is beryllium, $\kappa_{0He}/\kappa_{0W} \approx 0.27$. Then

$$B \approx A\kappa_W/\kappa_{He}, \quad x_0 \approx 1/\kappa_W. \quad (\text{A10})$$

2. Sewing at $x = d_{He}$

The boundary conditions for the wave functions (5) and (7) at the point $x = d_{He}$ are written as

$$\psi(d_{He} - 0) = \psi(d_{He} + 0); \quad \psi'(d_{He} - 0) = \psi'(d_{He} + 0) \quad (\text{A11})$$

and give

$$B \sinh[\kappa_{He}(d_{He} + x_0)] = C \sin[k(d_{He} + x_1)], \quad (\text{A12})$$

$$B\kappa_{He} \cosh[\kappa_{He}(d_{He} + x_0)] = Ck \cos[k(d_{He} + x_1)] \quad (\text{A13})$$

One can relate the coefficients B and C without calculating x_1 , using the trigonometric identity

$$1 = (B \sinh [\kappa_{He} (d_{He} + x_0)] / C)^2 + (B \kappa_{He} \cosh [\kappa_{He} (d_{He} + x_0)] / C k)^2, \quad (\text{A14})$$

which gives

$$C = B \left\{ (\sinh [\kappa_{He} (d_{He} + x_0)])^2 + (\cosh [\kappa_{He} (d_{He} + x_0)] \kappa_{He} / k)^2 \right\}^{1/2}. \quad (\text{A15})$$

Using Eqs. (A8) and (A15), we obtain Eq. (8).

The shift x_1 can be found from the ratio of Eqs. (A12) and (A13):

$$k \tanh [\kappa_{He} (d_{He} + x_0)] = \kappa_{He} \tan [k (d_{He} + x_1)], \quad (\text{A16})$$

which gives Eq. (11).

-
- * grigorev@itp.ac.ru
- [1] H. Abele, *Progress in Particle and Nuclear Physics* **60**, 1 (2008).
- [2] M. Ramsey-Musolf and S. Su, *Physics Reports* **456**, 1 (2008).
- [3] D. Dubbers and M. G. Schmidt, *Rev. Mod. Phys.* **83**, 1111 (2011).
- [4] F. E. Wietfeldt and G. L. Greene, *Rev. Mod. Phys.* **83**, 1173 (2011).
- [5] M. González-Alonso, O. Naviliat-Cuncic, and N. Severijns, *Progress in Particle and Nuclear Physics* **104**, 165 (2019).
- [6] M. Pospelov and A. Ritz, *Annals of Physics* **318**, 119 (2005), special Issue.
- [7] C. A. Baker, D. D. Doyle, P. Geltenbort, K. Green, M. G. D. van der Grinten, P. G. Harris, P. Iaydjiev, S. N. Ivanov, D. J. R. May, J. M. Pendlebury, J. D. Richardson, D. Shiers, and K. F. Smith, *Phys. Rev. Lett.* **97**, 131801 (2006).
- [8] A. P. Serebrov, E. A. Kolomenskiy, A. N. Pirozhkov, I. A. Krasnoschekova, A. V. Vassiljev, A. O. Polushkin, M. S. Lasakov, A. K. Fomin, I. V. Shoka, V. A. Solovey, O. M. Zherebtsov, P. Geltenbort, S. N. Ivanov, O. Zimmer, E. B. Alexandrov, S. P. Dmitriev, and N. A. Dovator, *JETP Letters* **99**, 4 (2014).
- [9] B. Märkisch, H. Mest, H. Saul, X. Wang, H. Abele, D. Dubbers, M. Klopff, A. Petoukhov, C. Roick, T. Soldner, and D. Werder, *Phys. Rev. Lett.* **122**, 242501 (2019).
- [10] J. Liu, M. P. Mendenhall, A. T. Holley, H. O. Back, T. J. Bowles, L. J. Broussard, R. Carr, S. Clayton, S. Currie, B. W. Filippone, A. García, P. Geltenbort, K. P. Hickerson, J. Hoagland, G. E. Hogan, B. Hona, T. M. Ito, C.-Y. Liu, M. Makela, R. R. Mammei, J. W. Martin, D. Melconian, C. L. Morris, R. W. Pattie, A. Pérez Galván, M. L. Pitt, B. Plaster, J. C. Ramsey, R. Rios, R. Russell, A. Saunders, S. J. Seestrom, W. E. Sondheim, E. Tatar, R. B. Vogelaar, B. VornDick, C. Wrede, H. Yan, and A. R. Young (UCNA Collaboration), *Phys. Rev. Lett.* **105**, 181803 (2010).
- [11] X. Sun, E. Adamek, B. Algeier, Y. Bagdasarova, D. B. Berguno, M. Blatnik, T. J. Bowles, L. J. Broussard, M. A.-P. Brown, R. Carr, S. Clayton, C. Cude-Woods, S. Currie, E. B. Dees, X. Ding, B. W. Filippone, A. García, P. Geltenbort, S. Hasan, K. P. Hickerson, J. Hoagland, R. Hong, A. T. Holley, T. M. Ito, A. Knecht, C.-Y. Liu, J. Liu, M. Makela, R. Mammei, J. W. Martin, D. Melconian, M. P. Mendenhall, S. D. Moore, C. L. Morris, S. Nepal, N. Nouri, R. W. Pattie, A. Pérez Galván, D. G. Phillips, R. Picker, M. L. Pitt, B. Plaster, D. J. Salvat, A. Saunders, E. I. Sharapov, S. Sjøe, S. Slutsky, W. Sondheim, C. Swank, E. Tatar, R. B. Vogelaar, B. VornDick, Z. Wang, W. Wei, J. W. Wexler, T. Womack, C. Wrede, A. R. Young, and B. A. Zeck (UCNA Collaboration), *Phys. Rev. C* **101**, 035503 (2020).
- [12] V. V. Nesvizhevsky, H. G. Börner, A. K. Petukhov, H. Abele, S. Baeßler, F. J. Rueß, T. Stöferle, A. Westphal, A. M. Gagarski, G. A. Petrov, and A. V. Strelkov, *Nature* **415**, 297 (2002).
- [13] T. Jenke, G. Cronenberg, J. Burgdörfer, L. A. Chizhova, P. Geltenbort, A. N. Ivanov, T. Lauer, T. Lins, S. Rotter, H. Saul, U. Schmidt, and H. Abele, *Phys. Rev. Lett.* **112**, 151105 (2014).
- [14] R. Golub, D. Richardson, and L. S.K., *Ultra-Cold Neutrons* (CRC Press, 1991).
- [15] V. Ignatovich, *The Physics of Ultracold Neutrons* (Clarendon Press, 1990).
- [16] V. K. Ignatovich, *Physics-Uspekhi* **39**, 283 (1996).
- [17] A. P. Serebrov, V. E. Varlamov, A. G. Kharitonov, A. K. Fomin, Y. N. Pokotilovski, P. Geltenbort, I. A. Krasnoschekova, M. S. Lasakov, R. R. Taldaev, A. V. Vassiljev, and O. M. Zherebtsov, *Phys. Rev. C* **78**, 035505 (2008).
- [18] S. Arzumanov, L. Bondarenko, S. Chernyavsky, P. Geltenbort, V. Morozov, V. Nesvizhevsky, Y. Panin, and A. Strepetov, *Physics Letters B* **745**, 79 (2015).
- [19] A. P. Serebrov, E. A. Kolomenskiy, A. K. Fomin, I. A. Krasnoschekova, A. V. Vassiljev, D. M. Prudnikov, I. V. Shoka, A. V. Chechkin, M. E. Chaikovskii, V. E. Varlamov, S. N. Ivanov, A. N. Pirozhkov, P. Geltenbort, O. Zimmer, T. Jenke, M. Van der Grinten, and M. Tucker, *JETP Letters* **106**, 623 (2017).
- [20] A. P. Serebrov, E. A. Kolomenskiy, A. K. Fomin, I. A. Krasnoschekova, A. V. Vassiljev, D. M. Prudnikov, I. V. Shoka, A. V. Chechkin, M. E. Chaikovskiy, V. E. Varlamov, S. N. Ivanov, A. N. Pirozhkov, P. Geltenbort, O. Zimmer, T. Jenke, M. Van der Grinten, and M. Tucker, *Phys. Rev. C* **97**, 055503 (2018).
- [21] Pattie, R.W., Callahan, N.B., Cude-Woods, C., Adamek, E.R., Adams, M., Barlow, D., Blatnik, M., D., Bowman, Broussard, L.J., Clayton, S., Currie, S., Dees, E.B., Ding, X., Fellers, D., Fox, W., Fries, E., Gonzalez, F., Geltenbort, P., Hickerson, K.P., Hoffbauer, M.A., Hoffman, K., Holley, A.T., Howard, D., Ito, T.M., Komives, A., Liu, C.Y., M., Makela, Medina, J., Morley, D., Morris, C.L., O'Connor, T., Penttilä, S.I., Ramsey, J.C., Roberts, A., Salvat, D., Saunders, A., Seestrom, S.J., Sharapov, E.I., Sjøe, S.K.L., Snow, W.M., Sprow, A., Vanderwerp,

- J., Vogelaar, B., P.L., Walstrom, Wang, Z., Weaver, H., Wexler, J., Womack, T.L., Young, A.R., and Zeck, B.A., EPJ Web Conf. **219**, 03004 (2019).
- [22] P. R. Huffman, C. R. Brome, J. S. Butterworth, K. J. Coakley, M. S. Dewey, S. N. Dzhosyuk, R. Golub, G. L. Greene, K. Habicht, S. K. Lamoreaux, C. E. H. Mattioni, D. N. McKinsey, F. E. Wietfeldt, and J. M. Doyle, Nature **403**, 62 (2000).
- [23] K. K. H. Leung, P. Geltenbort, S. Ivanov, F. Rosenau, and O. Zimmer, Phys. Rev. C **94**, 045502 (2016).
- [24] A. Steyerl, K. K. H. Leung, C. Kaufman, G. Müller, and S. S. Malik, Phys. Rev. C **95**, 035502 (2017).
- [25] V. F. Ezhov, A. Z. Andreev, G. Ban, B. A. Bazarov, P. Geltenbort, A. G. Glushkov, V. A. Knyazkov, N. A. Kovrizhnykh, G. B. Krygin, O. Naviliat-Cuncic, and V. L. Ryabov, JETP Letters **107**, 671 (2018).
- [26] R. W. Pattie, N. B. Callahan, C. Cude-Woods, E. R. Adamek, L. J. Broussard, S. M. Clayton, S. A. Currie, E. B. Dees, X. Ding, E. M. Engel, D. E. Fellers, W. Fox, P. Geltenbort, K. P. Hickerson, M. A. Hoffbauer, A. T. Holley, A. Komives, C.-Y. Liu, S. W. T. MacDonald, M. Makela, C. L. Morris, J. D. Ortiz, J. Ramsey, D. J. Salvat, A. Saunders, S. J. Seestrom, E. I. Sharapov, S. K. Sjue, Z. Tang, J. Vanderwerp, B. Vogelaar, P. L. Walstrom, Z. Wang, W. Wei, H. L. Weaver, J. W. Wexler, T. L. Womack, A. R. Young, and B. A. Zeck, Science **360**, 627 (2018), <https://science.sciencemag.org/content/360/6389/627.full.pdf>
- [27] J. S. Nico, M. S. Dewey, D. M. Gilliam, F. E. Wietfeldt, X. Fei, W. M. Snow, G. L. Greene, J. Pauwels, R. Eykens, A. Lamberty, J. V. Gestel, and R. D. Scott, Phys. Rev. C **71**, 055502 (2005).
- [28] A. T. Yue, M. S. Dewey, D. M. Gilliam, G. L. Greene, A. B. Laptev, J. S. Nico, W. M. Snow, and F. E. Wietfeldt, Phys. Rev. Lett. **111**, 222501 (2013).
- [29] K. Hirota, G. Ichikawa, S. Ieki, T. Ino, Y. Iwashita, M. Kitaguchi, R. Kitahara, J. Koga, K. Mishima, T. Mogi, K. Morikawa, A. Morishita, N. Nagakura, H. Oide, H. Okabe, H. Otono, Y. Seki, D. Sekiba, T. Shima, H. M. Shimizu, N. Sumi, H. Sumino, T. Tomita, H. Uehara, T. Yamada, S. Yamashita, K. Yano, M. Yokohashi, and T. Yoshioka, Progress of Theoretical and Experimental Physics **2020**, 123C02, (2020). 10.1093/ptep/ptaa169.
- [30] S. Rajendran and H. Ramani, Phys. Rev. D **103**, 035014 (2021).
- [31] A. P. Serebrov, Physics-Uspekhi **62**, 596 (2019).
- [32] A. P. Serebrov, M. E. Chaikovskii, G. N. Klyushnikov, O. M. Zherebtsov, and A. V. Chechkin, Phys. Rev. D **103**, 074010 (2021).
- [33] D. Dubbers, H. Saul, B. Märkisch, T. Soldner, and H. Abele, Phys. Lett. B **791**, 6 (2019), arXiv:1812.00626 [nucl-ex].
- [34] P. Ageron, W. Mampe, and A. I. Kilvington, Zeitschrift für Physik B Condensed Matter **59**, 261 (1985).
- [35] Y. Y. Kosvintsev, V. I. Morozov, and G. I. Terekhov, JETP Lett. **44**, 571 (1986).
- [36] V. Morozov, Nuclear Instruments and Methods in Physics Research Section A: Accelerators, Spectrometers, Detectors and Associated Equipment **1768**, 1 (2010).
- [37] A. Kharitonov, V. Nesvizhevsky, A. Serebrov, R. Taldaev, V. Varlamov, A. Vasilyev, V. Alfimenkov, V. Lushchikov, V. Shvetsov, and A. Strelkov, Nuclear Instruments and Methods in Physics Research Section A: Accelerators, Spectrometers, Detectors and Associated Equipment **281**, 1 (2010).
- [38] W. Mampe, P. Ageron, C. Bates, J. M. Pendlebury, and A. Steyerl, Phys. Rev. Lett. **63**, 593 (1989).
- [39] A. Pichlmaier, V. Varlamov, K. Schreckenbach, and P. Geltenbort, Physics Letters B **693**, 221 (2010).
- [40] E. Goremychkin and Y. Pokotilovski, JETP Letters (2017).
- [41] S. Ahmed, E. Altieri, T. Andalib, B. Bell, C. P. Bidinosti, E. Cudmore, M. Das, C. A. Davis, B. Franke, M. Gericke, P. Giampa, P. Gnyp, S. Hansen-Romu, K. Hatanaka, T. Hayamizu, B. Jamieson, D. Jones, S. Kawasaki, T. Kikawa, M. Kitaguchi, W. Klassen, A. Konaka, E. Korkmaz, F. Kuchler, M. Lang, L. Lee, T. Lindner, K. W. Madison, Y. Makida, J. Mammei, R. Mammed, J. W. Martin, R. Matsumiya, E. Miller, K. Mishima, T. Momose, T. Okamura, S. Page, R. Picker, E. Pierre, W. D. Ramsay, L. Rebenitsch, F. Rehm, W. Schreyer, H. M. Shimizu, S. Sidhu, A. Sikora, J. Smith, I. Tanihata, B. Thorsteinson, S. Vanbergen, W. T. H. van Oers, and Y. X. Watanabe (TUCAN Collaboration9), Phys. Rev. C **99**, 025503 (2019).
- [42] O. Zimmer, Phys. Rev. C **93**, 035503 (2016).
- [43] P. C. Bokun, Sov. J. Nucl. Phys. **40**, 287 (1984).
- [44] V. P. V. P. Alfimenkov, V. K. Ignatovich, L. P. Mezhdoglin, V. I. Morozov, A. V. Strelkov, and P. M. I., Communications of Joint Institute for Nuclear Research, Dubna prep.
- [45] O. Zimmer and R. Golub, Phys. Rev. C **92**, 015501 (2015).
- [46] P. D. Grigoriev, O. Zimmer, A. D. Grigoriev, and T. Ziman, Phys. Rev. C **94**, 025504 (2016).
- [47] L. Landau and E. Lifshitz, *Quantum Mechanics: Non-Relativistic Theory*, Course of theoretical physics (Elsevier Science, 1991).
- [48] K. R. Atkins and W. L. Bragg, Proceedings of the Royal Society of London. Series A. Mathematical and Physical Sciences.
- [49] E. J. Burge, L. C. Jackson, and N. F. Mott, Proceedings of the Royal Society of London. Series A. Mathematical and Physical Sciences.
- [50] R. Bowers, The London, Edinburgh, and Dublin Philosophical Magazine and Journal of Science.
- [51] K. Atkins, Progress in Low Temperature Physics **2**, 105 (1957).
- [52] E. S. Sabisky and C. H. Anderson, Phys. Rev. A **7**, 790 (1973).
- [53] D. B. Crum, D. O. Edwards, and R. E. Sarwinski, Phys. Rev. A **9**, 1312 (1974).
- [54] E. M. Lifshitz, Sov. Phys. JETP **2**, 73 (1956).
- [55] L. D. Landau and E. M. Lifshitz, *Fluid Mechanics, Second Edition: Volume 6 (Course of Theoretical Physics)*, 2nd ed., Course of theoretical physics / by L. D. Landau and E. M. Lifshitz, Vol. 6 (Butterworth-Heinemann, 1987).
- [56] A. Ham and L. Jackson, The London, Edinburgh, and Dublin Philosophical Magazine and Journal of Science.
- [57] D. Whitehouse, *Surfaces and their Measurement* (Elsevier Science, 2004).
- [58] Y. Bourgin, Y. Jourlin, O. Parriaux, A. Talneau, S. Tonchev, C. Veillas, P. Karvinen, N. Passilly, A. R. M. Zain, R. M. D. L. Rue, J. V. Erps, and D. Troadec, Opt. Express **18**, 10557 (2010).
- [59] V. Nesvizhevsky, R. Cubitt, E. Lychagin, A. Muzychka, G. Nekhaev, G. Pignol, K. Protasov, and A. Strelkov, Nuclear Instruments and Methods in Physics Research Section A: Accelerators, Spectrometers, Detectors and Associated Equipment **281**, 1 (2010).
- [60] G. Bison, M. Daum, K. Kirch, B. Lauss, D. Ries, P. Schmidt-Wellenburg, G. Zsigmond, T. Brenner, P. Geltenbort, T. Jenke, O. Zimmer, M. Beck, W. Heil, A. Caldehara, S. J. Kim, K. R. Pöschel, K. Elberhans, G. E. P. Pert, S. Karpuk, T. Reich, C. Siemensen, Y. Sobolev, and N. Trautmann, Phys. Rev. C **95**, 045503 (2017).

- [61] C. Jewell, R. Golub, and P. McClintock, *Cryogenics* **22**, 373 (1982).
- [62] P. Hendry and P. McClintock, *Cryogenics* **27**, 131 (1987).
- [63] M. E. Hayden, S. K. Lamoreaux, and R. Golub, *AIP Conference Proceedings* **850**, 147 (2006), <https://aip.scitation.org/doi/pdf/10.1063/1.2354645>.
- [64] K. Baumann, R. Gähler, P. Grigoriev, and E. I. Kats, *Phys. Rev. A* **72**, 043619 (2005).